J Opt (December 2023) 52(4):2366–2374
https://doi.org/10.1007/s12596-023-01167-0

RESEARCH ARTICLE

Effect of sintering temperature on structural and optical properties of magnesium aluminate spinel

Prabhpreet Kaur[1] · Suman Rani[1]

Received: 25 December 2022 / Accepted: 11 March 2023 / Published online: 25 March 2023

Abstract Magnesium aluminate spinel ($MgAl_2O_4$) (MAO) was fabricated by sol–gel process and sintered at a temperature ranging from 700 to 1400 °C. The phase development of MAO was confirmed by X-ray diffraction (XRD), Fourier transfer infrared spectroscopy (FTIR), and scanning electron microscopy. The XRD data confirms the formation of MAO spinel. FTIR analysis matches well with XRD data. The obtained results show that the optimized phase and morphology of the prepared nanoparticles were achieved at 1100 °C. The optical behavior of MAO was investigated using UV–Vis spectroscopy (UV–Vis) and fluorescence spectroscopy. Down-conversion energy transition from UV to visible light had been studied with three different excitations, 351 nm, 395 nm, and 405 nm. The material's color purity and CIE coordinates indicate that it is ideal for optoelectronic applications.

Keywords Spinel · Color purity · Energy transition · Down-conversion

Introduction

$MgAl_2O_4$ (MAO) spinel has the general formula XAl_2O_4 (where X = Mg) and is known as a key component of the spinel aluminate family. MAO can provide great stability to the structure against temperature, high energy radiation, and pressure. The melting point of MAO is very high (2135 °C) which makes it one of the essential refractory materials [1–3]. MAO is a mixed oxide having the physical properties of magnesium oxide and aluminum oxide. The physical and optical properties of the material depend upon the shape, size, nature of grain, grain boundaries, voids, orientation, and in-homogeneities present in the material [4, 5].

It had been reported in the literature that defects have a significant impact on the structural and optical properties of the material [6]. Defects play an important role in obtaining a good optical yield. The significant luminescence behavior is known to be induced by the presence of oxygen vacancies and other oxygen-related defects [7]. In addition, the presence of significant number of cations disorders in MAO (vacant 56 tetrahedral and 16 octahedral sites) allows the formation of intrinsic defects in the crystal which act as trapping centers for charge carriers [8, 9]. However, the formations of complex defects such as $V_0 + O_i$, $V_0 + Al_{Mg}$ and $V_0 + Mg_{Al}$ (where V_0 = oxygen vacancy, O_i = oxygen interstitial, Al_{Mg}&Mg_{Al} = antisites of aluminum and magnesium) might cause an optical transition [10, 11]. Borges [12] studied the native defects in $MgAl_2O_4$ which act as a source for optical transitions. Using the cathodoluminescence technique, Ghamnia et al. investigated the luminous centers (F and F+) in alumina [13]. Alumina material with a high density of defects is characterized by an increase in the intensity of F^+ emission and its response to irradiation time.

It has also been observed that the densification and sinterability of the material can be improved at lower temperatures since its strength qualities can be enhanced at higher temperatures [14–16]. In this study, MAO was prepared by sol–gel method and sintered at different temperatures from 700 to 1400 °C. The sol–gel method is a versatile technique for producing solid materials from small molecules, metal salts, or metal oxides dissolved in a liquid sol. The process involves several steps, including

✉ Suman Rani
suman.rani@lpu.co.in

[1] Department of Physics, School of Chemical Engineering and Physical Sciences, Lovely Professional University, Phagwara, Punjab 144411, India

the preparation of the sol, gelation, aging, and drying or calcination. The sol–gel method offers several advantages over other methods of material synthesis, such as high purity, good control over composition and structure, and the ability to produce a wide range of materials including ceramics, glasses, and composites. It is also a relatively simple and low-cost method, making it an attractive option for industrial-scale production.

Overall, the sol–gel method is a powerful tool for producing high-quality materials with tailored properties for a variety of applications, including catalysis, electronics, and optics.

The prepared material was characterized by XRD, UV–Vis, FTIR, SEM, and FL. The purpose of this study is to explore the effect of temperature on the structural and optical properties of magnesium aluminate spinel.

Experimental detail

Analytical reagent grade nitrate of magnesium Mg $(NO_3)_2{\cdot}6H_2O$ and aluminum Al $(NO_3)_3{\cdot}9H_2O$ was taken in a corresponding stoichiometric ratio, dissolved in deionized water. The solution was mixed at a temperature of 70 °C via the magnetic stirrer. After 3-h stirring, a chelating agent, citric acid ($C_6H_8O_7$) was added. The mixture was stirred until it gets the transparent viscous solution. This viscous solution was converted into cream color gel which was dried at 150 °C to form a powder. Moreover, the prepared powder was grinded manually in mortar and pestle for 30 min. Finally, to obtain $MgAl_2O_4$ spinel the prepared sample was sintered at temperatures of 700 °C, 800 °C, 900 °C, 1000 °C, 1100 °C and 1400 °C. The characterizations were carried out by using XRD, FTIR, SEM, UV–Vis, and fluorescence spectra techniques.

Bruker equipment with Cu-Kα radiation ($\lambda = 1.54060$ Å) was used to record an X-ray diffraction (XRD) pattern for the prepared MAO powder in the 2θ range of 20°–80°. Fourier transform infrared (FTIR) spectrum from Perkin Elmer has a scanning range from 8300 to 350 cm^{-1} offering a resolution of 0.5 cm^{-1}. The prepared sample of FTIR spectra was obtained in the 400–4000 cm^{-1} range. SEM, from Jeol, which has an accelerating voltage of 0.1–30 kV is used to examine the morphology of the prepared material at 700 °C, 900 °C, 1100 °C, and 1400 °C. Shimadzu UV–Vis spectrophotometer (UV-1900i) was used to record the excitation spectrum of the prepared sample. Perkin Elmer's fluorescence spectroscopy which has a pulse xenon lamp was used to examine the optical properties or emission properties of prepared material.

Results and discussion

Powder X-ray diffraction (XRD) analysis

Figure 1a illustrates the XRD spectra for magnesium aluminate spinel sintered at 700 °C, 800 °C, 900 °C, 1000 °C, 1100 °C, and 1400 °C temperatures recorded in the range of 20°–70° of Bragg's angle (2θ). In Fig. 1, no diffraction peaks were observed at 700 °C, indicating the amorphous nature of the material. At 800 °C, the crystalline phase started developing and consisted of mixed phases, but when the temperature was raised to 900 °C, the $MgAl_2O_4$ phase took dominance and it was found that the crystalline character improves as the sintering temperature increases. At a temperature of 1100 °C, the pure phase of MAO was found and peaks could be directly indexed to the cubic phase. So, these results designate that MAO configurations appear to be an established phase.

It can be observed that peak intensity increases with sintering temperature up to 1100 °C; however, around 1400 °C, the intensity of the peaks decreases slightly. The observed peaks have corresponding (*hkl*) planes (220), (311), (200), (400), (422), (511), (220), and (440). However, two additional peaks having (*hkl*) plane (200) and (220) are due to the presence of MgO phase [17]. Figure 1b shows the peak shifting of (311) and (200) peaks. The peak is shifting toward a lower angle, indicating that inter-planar distance is expanding [18].

The *d*-spacing (d), peak intensity, crystalline size (D), and lattice parameter *a* (Å) are tabulated in Table 1. Using Bragg's Law and the Scherrer equation, the *d*-spacing, crystallite size, and lattice parameter [peak corresponding to (311) plane] produced at different sintering temperatures were calculated. The material's porosity (*P*) is also determined using the XRD data. The value of porosity was calculated using the relation mention in Figure 2b. As the sintering temperature increases from 800 to 1400 °C, the porosity decreases from 0.96 to 0.93% due to the process of sintering densification. Decreasing the porosity of a material can have a significant impact on its optical properties, particularly when it comes to its emission properties. When a material is porous, it can trap light within its pores, leading to decreased emission efficiency. By reducing the porosity of the material, more of the emitted light can escape, resulting in an increase in emission

$$d = \frac{n\lambda}{2\sin\theta} \tag{1}$$

$$D = \frac{0.94\lambda}{\beta\cos\theta} \tag{2}$$

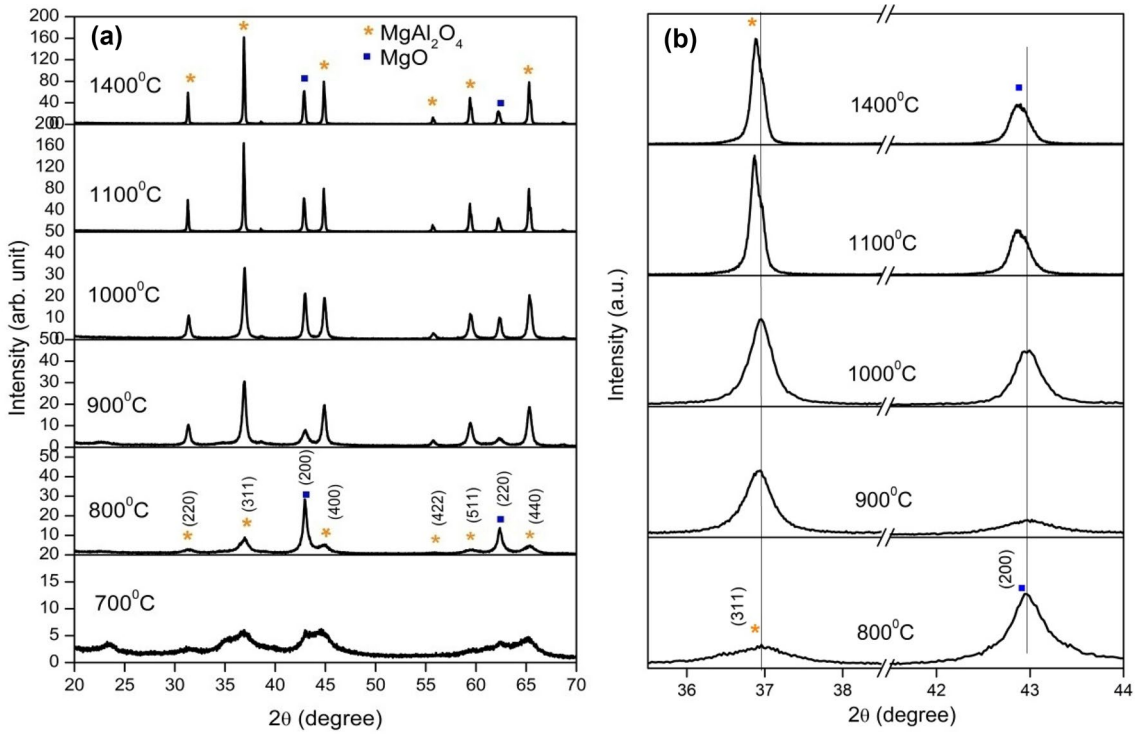

Fig. 1 The XRD pattern of $MgAl_2O_4$ **a** sintered at 700 °C, 800 °C, 900 °C, 1100 °C and 1400 °C **b** shift in 2θ with increase in sintering temperature

Table 1 Structure parameters of $MgAl_2O_4$ at different temperatures

	Temp. (°C)	2θ (°)	Peak intensity (A.U.)	Crystallite size (nm)	*d*-spacing (Å)	Lattice Parameter ($a=b=c$) (Å)	Porosity (%)
$MgAl_2O_4$	800	36.982	8.3071	8.46	2.4348	8.0753	0.96
	900	36.922	30.7750	22.19	2.4356	8.0781	0.95
	1000	36.946	33.3270	25.72	2.4310	8.0629	0.94
	1100	36.874	164.5900	49.42	2.4325	8.0679	0.94
	1400	36.887	160.7600	46.04	2.4287	8.0553	0.93

$$a = \left[d^2\left(h^2 + k^2 + l^2\right)\right]^{1/2} \tag{3}$$

Figure 2 shows the relation between peak shift and crystallite size as a function of sintering temperature. As the temperature rises, peaks shifted toward the lower angle side because of tensile strain. There was a uniform increase in crystallite size up to 1100 °C. The increase in peak shifts with crystallite size indicates the expansion of the lattice up to 1100 °C. However, the lattice starts to contract above 1100 °C temperature, as clearly seen in the graph. The peak shift observed in the XRD pattern may be related to the incomplete reaction and the presence of excess magnesium and oxygen, or it may be due to lattice strain caused by defects introduced during the reaction.

Scanning electron microscopy (SEM)

Figure 3 shows the SEM images of sintered $MgAl_2O_4$ at 700 °C, 900 °C, 1100 °C, and 1400 °C temperatures. From the SEM images, it is observed that the particle size and surface morphology behave differently with rising temperatures. At 700 °C material was amorphous in nature as shown in Fig. 3a. At 900 °C, crystalline nature starts developing in the material and particles become indistinguishable (Fig. 3b). It can be seen that with the increase

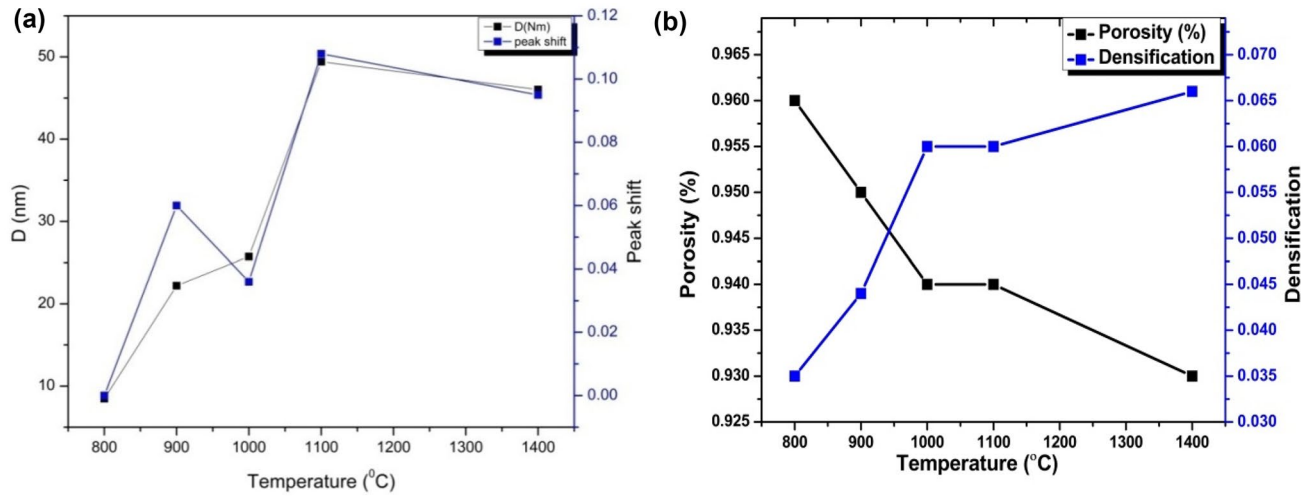

Fig. 2 **a** Peak shift and crystallite size as a function of sintering temperature. **b** variation of porosity and densification

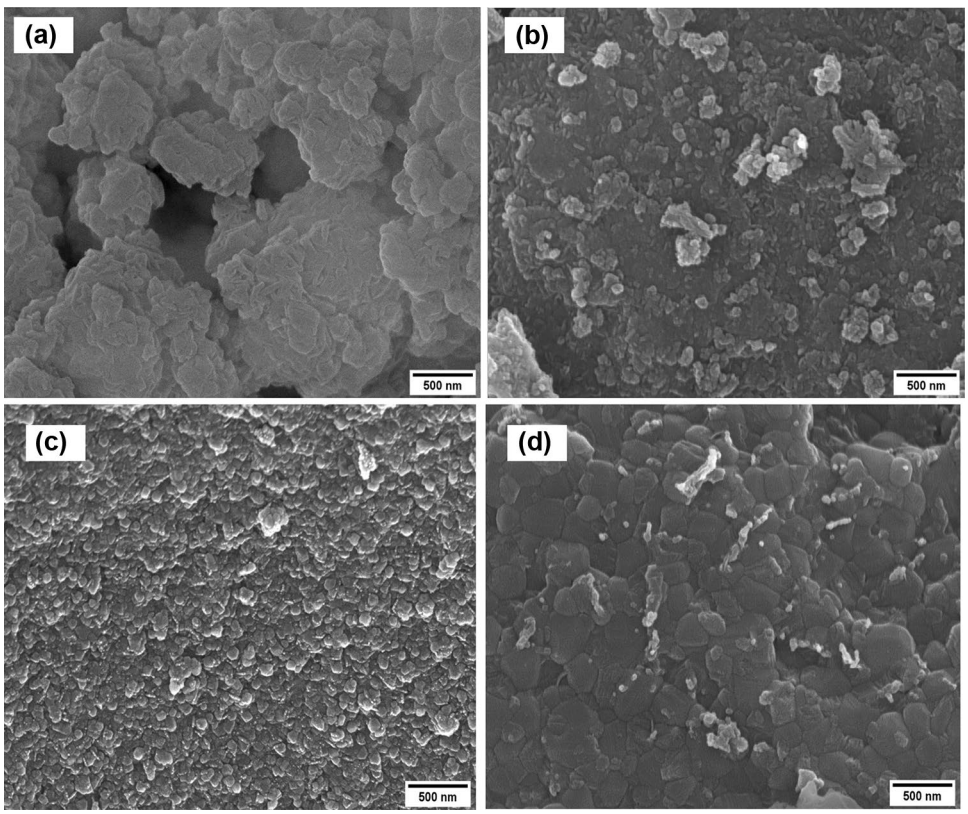

Fig. 3 SEM images of MAO at **a** 700 °C **b** 900 °C **c** 1100 °C **d** 1400 °C

in sintering temperature, the size of the crystallites also increases. With increases in temperatures, the shape of the crystallites was smooth and rounded, forming irregular structures. With the increase in the temperature, the crystallites sinter together and form larger grains and aggregates. The distribution of the grain size varied, and for the highest calcination temperature, at 1100 °C fine- and irregular-shaped crystal particles were formed and the average particle size calculated from SEM is around 62 nm which also verified the XRD results. Moreover, on a further increase in temperature up to 1400 °C, the particles started to take on an irregular shape and size, and agglomeration particles appeared. The particle size calculation was done by taking forty selected particles from each image as shown in Fig. 4.

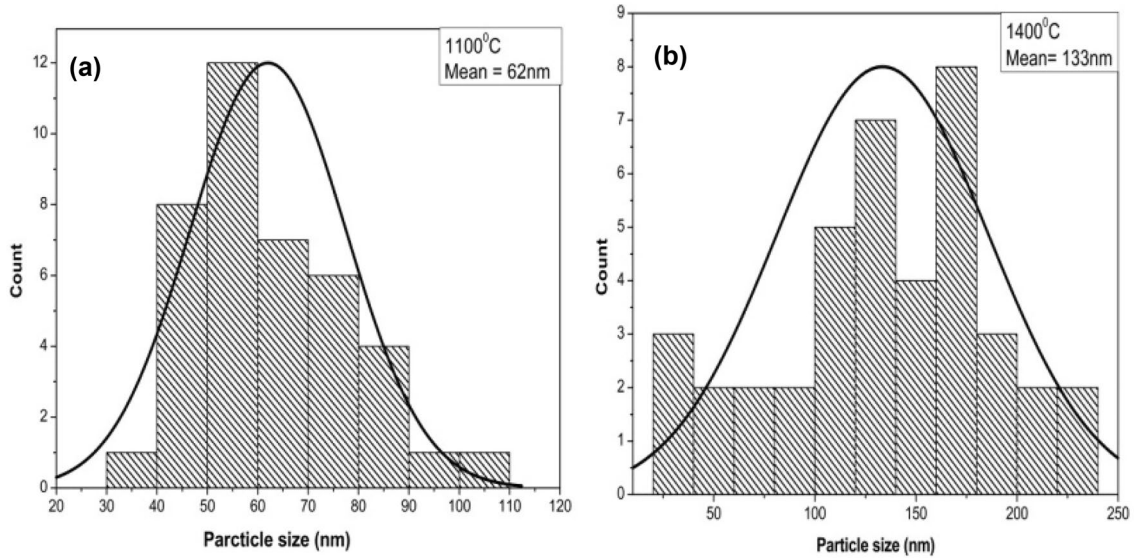

Fig. 4 Particle size of MAO at sintering temperature of **a** 1100 °C **b** 1400 °C

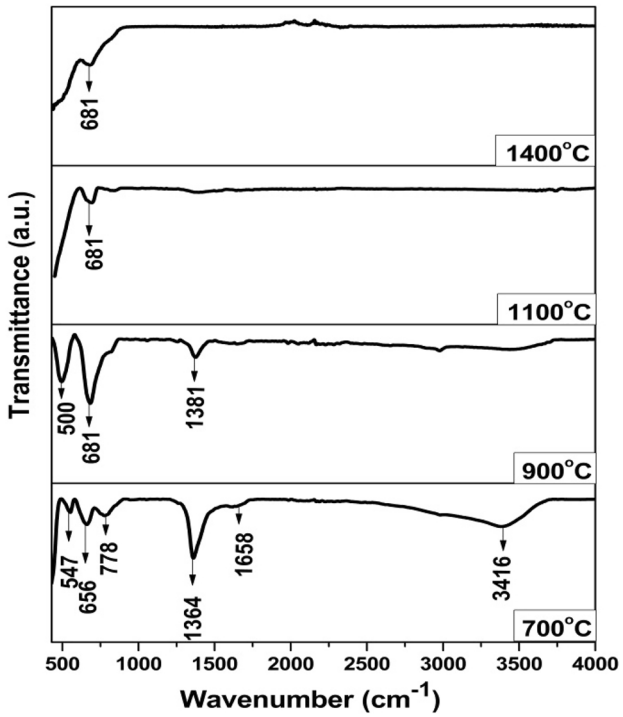

Fig. 5 FTIR spectra of MAO at different sintering temperatures

Fourier transfer infrared spectroscopy (FTIR)

The FTIR spectra of prepared samples in the wavenumber range of 400–4000 cm^{-1} are shown in Fig. 5. The FTIR spectrum confirms the co-ordinance state of Al and Mg cations in the nanocrystalline spinel phase.

1. It is considered that at 700 °C the peak at wavenumber of 3416 cm^{-1} and at 1658 cm^{-1} was due to the –OH stretching and H–O–H bending vibrations of adsorbed water, respectively, which reflects the large surface area of the powder [19]. The intensity of these peaks vanished as the sintering temperature increases. In addition to this, the absorption band around 1364 cm^{-1} is attributed to the vibrations of N–O bond of NO^{3-} groups. The two peaks observed at 656 cm^{-1} and 547 cm^{-1} match the vibrations Mg–O–Al bond.
2. At 900 °C, peak observed at 1381 cm^{-1} indicates the presence of N–O (nitrates) vibrations. These vibrations of nitrates vanish with rise in temperature. The peaks present at 681 cm^{-1} and 500 cm^{-1} indicates the formation of $MgAl_2O_4$ spinel.
3. At low temperature, some impurity peaks were found; however, impurities get vanished with the rise in temperature as shown in Fig. 5. The water and nitrate peaks get disappeared with the rise in temperature. At higher temperatures, i.e., at 1100 °C and 1400 °C, only metal–oxygen–metal peaks of Mg–O–Al bonds appeared which successfully confirms the formation of $MgAl_2O_4$ spinel. The wavenumber with their corresponding functional group is mentioned in Table 2.

At all different temperatures 700 °C, 900 °C, 1100 °C, and 1400 °C, the metal–oxygen–metal bond is formed ranging from 500 to 800 cm^{-1}, as mentioned in Table 2. The vibration bands in this region point out the spinel-type structure, which is linked by the lattice vibrations of tetrahedral and octahedral coordinated metal ions [20]. This spectral region from 500 to 800 cm^{-1} is vibrational Al–O bonds

Table 2 Wavenumbers and related functional groups in FTIR spectra of MAO

Wavenumber	Functional group
500	Al–O (stretching)
547	AlO_6 group
656	Al–O (stretching)
681	Mg–O
778	AlO_4 (stretching)
1364, 1381	Vibration modes of nitrates
1658	Vibrations of H–O–H bonds
3416	–OH band

of the octahedral site and the network vibrations of Mg–O bonds occupied in normal spinel [21, 22]. The XRD and FTIR spectrum confirms the formation of $MgAl_2O_4$ spinel.

UV–Vis spectroscopy

UV–Vis absorption spectrum of MAO samples has been recorded with Shimazu 1800 UV–Vis spectrophotometer. UV–Vis spectroscopy was used to investigate the absorption properties of MAO spinel sintered at 900 °C, 1100 °C, and 1400 °C. Figure 6 shows the absorption spectrum consisting of absorption peaks around 299 nm, 310 nm, and 300 nm which indicate the existence of different kinds of defect states within the bandgap. The peaks at 299 nm and 310 nm can be assigned as F_2 and F_2^{2+} centers [23]. On the other hand, the band that appeared near the visible light region possibly will be attributed to the $O^{2-} \rightarrow Al^{3+}$ charge transition due to the excitation of electrons from the valance band of O (2*p*) to the conduction band of Al (3*d*) [24].

Fluorescence spectroscopy

Figure 7a shows the schematic diagram for the excitation mechanism in $MgAl_2O_4$. Emission spectra with excitation wavelengths of 351 nm, 395 nm, and 405 nm signify the presence of oxygen vacancies. In the MAO compound, *p* states of Al, Mg, and O contribute to the upper part of the valence band, while *s* and *p* states of Mg and Al, contribute to the lower part of the conduction band. Figure 7b shows four types of transition that take place after the

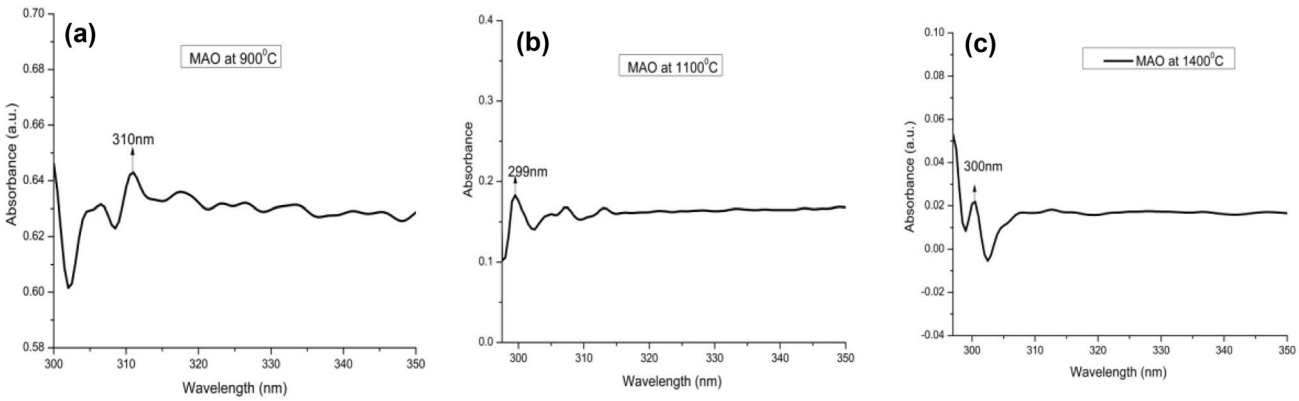

Fig. 6 The UV absorption of MAO at **a** 900 °C **b** 1100 °C **c**1400 °C

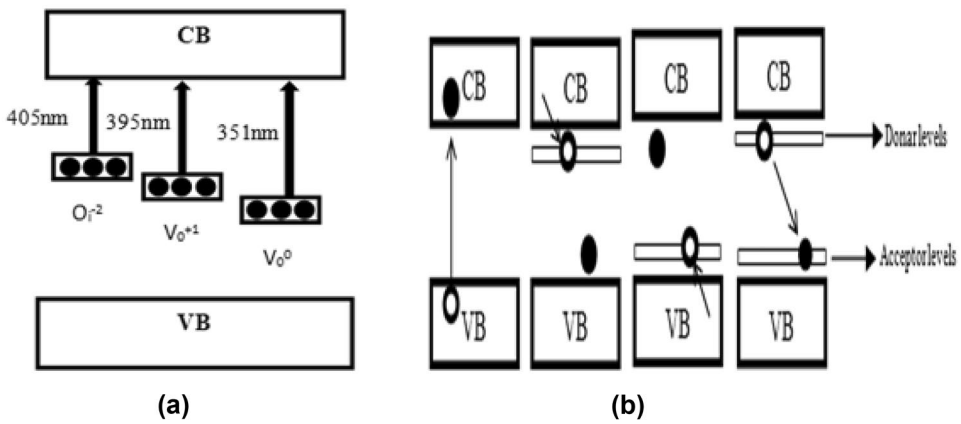

Fig. 7 **a** Excitation mechanism of MAO **b** Transition mechanism in MAO

photoionization process: (1) formation of an electron–hole pair by excitation of electrons from the valence band (VB) to the conduction band (CB); (2) electron transfer from the conduction band to the positively charged donor level just below the CB; (3) transition from the capture of the VB hole by the negatively charged acceptor level just above the VB; and (4) the transfer of a captured electron from the donor level to the acceptor level [25].

The fluorescence spectra of material prepared at higher temperatures were excited using three different excitation wavelengths, and it shows a broad emission band, as seen in Fig. 8. The compound reported in Table 3 has several emitting components that are responsible for broad emission profiles. From Table 3, it was observed emission efficiency increases with temperature supported the fact stated in XRD section that decreasing the porosity of a material can have a significant impact on its optical properties, particularly when it comes to its emission properties. When a material is porous, it can trap light within its pores, leading to decreased emission efficiency. By reducing the porosity of the material, more of the emitted light can escape, resulting in an increase in emission.

The charge transfer transition between Al^{3+} and its surrounding O^{2-} ions is responsible for the emission observed near 460 nm. The transition of an electron to a hole trapped at the Mg ion vacancy caused the green emission peaks around 490 nm [26, 27]. The peak at 525 nm is due to the presence of Oxygen vacancies [7]. The presence of F-centers causes peaks at 540 nm. F_2^{2+} centers surround the octahedralAl^{3+} ion, which is a pair of F^+ centers [28, 29], whereas a peak at 610 nm can be attributed to oxygen vacancies caused by the presence of Mg_{Al} antisites [30]. The peaks around 680 nm could be due to the presence of F_2^{1+} defect centers [31]. These multicolor emissions show the presence of multiple defect states inside the bandgap, each of which is caused by a different electronic transition. The occurrence of multiple defect states is the source of these electrical states [31]. It is also observed that the emission spectra do not change substantially when the MAO compound is sintered at higher temperatures. The integrated area under the curve with different sintering temperatures is compared in Table 4.

Table 3 Defects centers responsible for emission wavelength

S. no	Sample preparation temperature (°C)	Excitation wavelength (nm)	Integrated area under the curve (A.U.)
1	900	351	4256.25
	1100		3865.08
	1400		4650.45
2	900	391	3176.79
	1100		3141.99
	1400		2632.81
3	900	405	2403.43
	1100		3341.50
	1400		3368.91

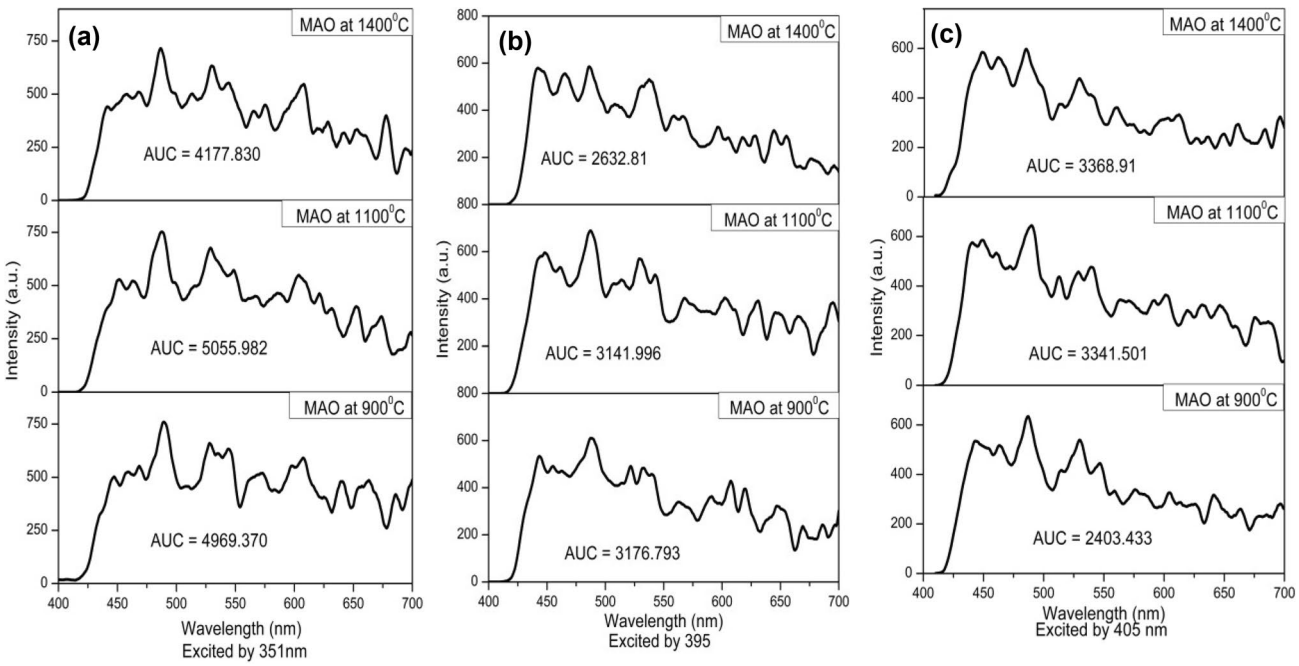

Fig. 8 Emission spectra of MAO excited by **a** 351 nm **b** 395 nm **c** 405 nm

Table 4 The excitation wavelength with an integrated area under the curve

Dominating emission wavelengths (nm)	Defects responsible for emission wavelength
460	Charge transfer between Al^{3+} and O^{2-}
490	Trapping of hole at Mg ion vacancy
525	Oxygen vacancy
540	F-centers
560	F_2^{2+}
610	Oxygen vacancy
680	F_2^{1+}

To denote the color characteristics of the prepared material, the CIE (Commission Internationale de I'Eclairage) coordinates were calculated. MAO at 900 °C, 1100 °C and 1400 °C was tested for white light source material by calculating color purity, CCT, and CIE coordinates. For an ideal white light source, CIE coordinates (x, y) should be close to (0.33, 0.33) and color purity close to zero. CCT (color correlated temperature) theoretical parameter compares the appearance of the light emitted by a light source with a black body as a reference source when heated to a particular temperature in degrees Kelvin (K). If the CCT value is more than 3200 K, then light is warm (yellow) and usually less than 4000 K which is cool light (blue). The values of x and y coordinates indicate that the material has the potential to use a white light-emitting source. The color purity of these phosphors is calculated using the equation:

$$\text{color purity} = \frac{\sqrt{(x_s - x_i)^2 + (y_s - y_i)^2}}{\sqrt{(x_d - x_i)^2 + (y_d - y_i)^2}} \times 100\%$$

where (x_i, y_i) is the CIE coordinates for white light, (x_s, y_s) is the chromaticity coordinates of prepared phosphors, and (x_d, y_d) is the chromaticity coordinates of the dominant wavelength. The calculated value of color purity, CCT, and CIE coordinates of the MAO sample prepared at 900 °C, 1100 °C, and 1400 °C is tabulated in Table 5.

Conclusion

MAO spinel was sintered at temperatures ranging from 700 to 1400 °C using the sol–gel method. The XRD analysis revealed a uniform increase in crystallite size up to 1100 °C, indicating lattice expansion, and then contracting at 1400 °C. SEM images concluded that particle size and surface morphology behave differently with increased temperatures. Peaks in the UV absorption spectra around 299 nm, 310 nm, and 300 nm indicate the presence of several kinds of defect states in the bandgap. MAO sintered at 1100 °C produces the best results with 395 nm excitation, with CIE coordinates, color purity, and CCT of (0.30, 0.33), 9.29, and 7214 K, confirming MAO as a good white light optical material.

Table 5 The calculated value of CIE coordinates, CCT, and color purity of MAO sample sintered at 900 °C, 1100 °C, and 1400 °C with excitation wavelengths 351,395 and 405 nm

S. no	Excitation wavelength (nm)	Sample (°C)	CIE coordinates	CCT (K)	Color purity (R)
1	351	900	(0.333, 0.365)	5484.59	10.309
		1100	(0.325, 0.369)	5779.90	10.302
		1400	(0.318, 0.363)	6081.54	14.96
2	395	900	(0.301, 0.329)	7167.58	8.85
		1100	(0.30, 0.332)	7213.91	9.29
		1400	(0.284, 0.328)	8236.97	12.24
3	405	900	(0.289, 0.326)	7751.91	14.70
		1100	(0.292, 0.314)	4286.99	12.38
		1400	(0.287, 0.314)	8422.85	14.94

Acknowledgements Authors would like to acknowledge Central Instrumental Facility (CIF) and Laboratories of Lovely Professional University for preparation of samples and carrying out all characterization.

References

1. W. Tsai, Y. Liou, Y. Liou, Microwave dielectric properties of $MgAl_2O_4$–$CoAl_2O_4$ spinel compounds prepared by reaction-sintering process. Mater. Sci. Eng. B **177**(13), 1133–1137 (2012)
2. S. Angappan, L. Berchmans, C. Augustin, Sintering behavior of $MgAl_2O_4$—a prospective anode material. Mater. Lett. **58**(17), 2283–2289 (2004)
3. H. Li, H. Wei, Y. Cui, R. Sang, J. Bu, Y. Wei, J. Lin, J. Zhao, Synthesis and characterisation of $MgAl_2O_4$ spinel nanopowders via nonhydrolytic sol–gel route. J. Ceram. Soc. Jpn. **125**(3), 100–104 (2017)
4. M. Park, J. Kim, K. Kim, J. Lee, J. Kim, Y. Yamauchi, Porous nanoarchitectures of spinel-type transition metal oxides for electrochemical energy storage systems. Phys. Chem. Chem. Phys. **17**(46), 30963–30977 (2015)
5. B. Goswami, N. Rani, R. Vats, C. Bhukkal, R. Ahlawat, Highly crystalline and narrow bandgap $MgAl_2O_4$: synthesis and characterization. AIP Conf. Proc. **2352**(1), 020045 (2021)
6. N. Pathak, B. Sanyal, S. Gupta, R. Kadam, $MgAl_2O_4$ both as short and long persistent phosphor material: role of antisite defect centers in determining the decay kinetics. Solid State Sci. **88**, 13–19 (2019)
7. S. Raj, S. Gupta, V. Grover, K. Muthe, V. Natarajan, A. Tyagi, $MgAl_2O_4$ spinel: synthesis, carbon incorporation and defect-induced luminescence. J. Mol. Struct. **1089**, 81–85 (2015)
8. E. Yoshimura, E. Yukihara, Optically stimulated luminescence of magnesium aluminate ($MgAl_2O_4$) spinel. Radiat. Meas. **41**(2), 163–169 (2006)
9. Y. Hao, K. Wu, Investigation of the structural, morphological and luminescence properties of $MgAl_2O_4$:Cr^{3+} nano powders. J. Mater. Sci. Mater. Electron **30**(14), 13151–13157 (2019)
10. S. Murphy, C. Gilbert, R. Smith, T. Mitchell, R. Grimes, Non-stoichiometry in $MgAl_2O_4$ spinel. Philos. Mag. **90**(10), 1297–1305 (2010)
11. J. Spitaler, S. Estreicher, Perspectives on the theory of defects. Front. Mater. Sci. **5**, 70 (2018)
12. P. Borges, J. Cott, F. Pinto, J. Tronto, L. Scolfaro, Native defects as sources of optical transitions in $MgAl_2O_4$ spinel. Mater. Res. Express **3**(7), 076202 (2016)
13. M. Ghamnia, C. Jardin, M. Bouslama, Luminescent centres F and F+ in α-alumina detected by cathodoluminescence technique. J. Electron Spectrosc. Relat. Phenom. **133**(1), 55–63 (2003)
14. Y. Wen, X. Liu, X. Chen, Q. Jia, R. Yu, T. Ma, Effect of heat treatment conditions on the growth of $MgAl_2O_4$ nanoparticles obtained by sol-gel method. Ceram. Int. **43**(17), 15246–15253 (2017)
15. M. Khezrabad, M. Brauliob, V. Pandolfelli, F. Fard, H. Rezaie, Nano-bonded refractory castables. Ceram. Int. **39**(4), 3479–3497 (2013)
16. J. Werner, J. Fruhstorfer, A. Mertke, C. Ode, C. Aneziris, The influence of nano scaled additions on the Young's modulus of carbon-bonded alumina at temperatures up to 1450°C. Ceram. Int. **42**(14), 15718–15724 (2016)
17. C. Tang, Z. Zhai, X. Li, L. Sun, W. Bai, Sustainable production of acetaldehyde from lactic acid over the magnesium aluminate spinel. J. Taiwan Inst. Chem. Eng. **58**, 97–106 (2016)
18. T. Sawabe, M. Akiyoshi, K. Yoshida, T. Yano, Estimation of neutron-irradiation-induced defect in 3C–SiC from change in XRD peak shift and DFT study. J. Nucl. Mater. **417**(1), 430–434 (2011)
19. P. Lee, H. Suematsu, T. Yano, K. Yatsui, Synthesis and characterization of nanocrystalline $MgAl_2O_4$ spinel by polymerized complex method. J. Nanopart. Res. **8**(6), 911–917 (2006)
20. K. Waldner, R. Laine, S. Dhumrongvaraporn, S. Tayaniphan, R. Narayanan, Synthesis of a double alkoxide precursor to spinel ($MgAl_2O_4$) directly from $Al(OH)_3$, MgO, and triethanolamine and its pyrolytic transformation to spinel. Chem. Mater. **8**(12), 2850–2857 (1996)
21. T. Hinklin, R. Laine, Synthesis of metastable phases in the magnesium spinel–alumina system. Chem. Mater. **20**(2), 553–558 (2008)
22. P. Thibaudeau, F. Gervais, Ab initio investigation of phonon modes in the $MgAl_2O_4$ spinel. J. Phys. Condens. Matter. **14**(13), 3543 (2002)
23. A. Popov, L. Shirmane, V. Pankratov, A. Lushchik, A. Kotlov, V. Serga, L. Kulikova, G. Chikvaidze, J. Zimmermann, Comparative study of the luminescence properties of macro-and nanocrystalline MgO using synchrotron radiation. Nucl. Instrum. Methods Phys. Res. **310**, 23–26 (2013)
24. M. Nassar, I. Ahmed, I. Samir, A novel synthetic route for magnesium aluminate ($MgAl_2O_4$) nanoparticles using sol–gel auto combustion method and their photocatalytic properties. Spectrochim. Acta A Mol. Biomol. Spectrosc. **131**, 329–334 (2014)
25. F. Shahid, B. Ismail, A. Khan, Q. Ain, R. Khan, F. Shah, T. Fazal, M. Asghar, Cost effective way of tuning physical properties of $MgAl_2O_4$ spinel nanomaterials by Sr^{+2}/Mn^{2+} cations doped at the T-Sites. Ceram. Int. **46**(8), 10710–10717 (2020)
26. J. Kim, H. Kang, W. Kim, J. Kim, J. Choi, H. Park, G. Kim, T. Kim, Y. Hwang, S. Mho, M. Jung, Color variation of $ZnGa_2O_4$ phosphor by reduction–oxidation processes. Appl. Phys. Lett. **82**(13), 2029–2031 (2003)
27. J. Salmones, J. Galicia, J. Wang, M. Valenzuela, G. Aguilar, Synthesis and characterization of nanocrystallite $MgAl_2O_4$ spinels as catalysts support. J. Mater. Sci. Lett. **19**, 1033–1037 (2000)
28. M. Springis, J. Valbis, Visible luminescence of colourcentres in sapphire. Phys. Status Solidi B **123**(1), 335–343 (1984)
29. B. Evans, M. Stapelbroek, Optical vibronic absorption spectra in 14.8 MeV neutron damaged sapphire. Solid State Commun. **33**(7), 765–770 (1980)
30. L. Cornu, M. Gaudon, V. Jubera, $ZnAl_2O_4$ as a potential sensor: variation of luminescence with thermal history. J. Mater. Chem. C **1**(34), 5419–5428 (2013)
31. N. Pathak, P. Ghosh, S. Gupta, R. Kadam, A. Arya, Defects induced changes in the electronic structures of MgO and their correlation with the optical properties: a special case of electron–hole recombination from the conduction band. RSC Adv. **6**(98), 96398–96415 (2016)